

Pure dephasing of double-quantum-dot charge qubits in freestanding slabs

Y. Y. Liao^{1,*} and Y. N. Chen²

¹*Department of Applied Physics, National University of Kaohsiung, Kaohsiung 811, Taiwan*

²*Department of Physics and National Center for Theoretical Sciences, National Cheng-Kung University, Tainan 701, Taiwan*

(Received 7 October 2009; revised manuscript received 13 January 2010; published 1 April 2010)

We study phonon-induced pure dephasing in a double-quantum-dot qubit that is embedded in a freestanding slab. The dispersion relations are evaluated to probe the phonon characteristics of the slab. The pure dephasing factor in the off-diagonal elements of the density matrix is calculated. Numerical results demonstrate that time evolution of this factor exhibits a nonmonotonic feature, resulting from the phonon confinement effect. Significant contribution from individual phonon mode is analyzed in detail. We also study effects of temperature and double-dot position on the pure dephasing. In particular, two remarkable oscillations are observed due to phonon van Hove singularities.

DOI: [10.1103/PhysRevB.81.153301](https://doi.org/10.1103/PhysRevB.81.153301)

PACS number(s): 73.21.La, 63.22.-m, 71.38.-k, 03.65.Yz

The quantum dynamics of electrons in quantum dots has been widely studied for implementations of quantum computation and quantum information processing.¹⁻³ The nanostructured platforms based on quantum dots possess an advantage of the direct controllability through external voltages.⁴ In addition, their large-scale integration and scalability are experimentally supported by advanced manufacturing technologies. Recently, double quantum dot (DQD) is considered to serve as a promising candidate to realize the structural function of a quantum bit (qubit) in solid-state devices.⁵ A two-level system can be established by employing charge degrees of freedom, namely, the locations of electron in the dots.³ Such a DQD charge qubit has been demonstrated in recent experiments.⁶⁻⁸

Quantum coherence is fundamentally important in the performance of the qubit.^{9,10} The number of quantum operations is strongly affected by the interaction between the quantum dot and its embedded environment. In fact, electron-phonon interaction is one of the major sources of decoherence.¹¹⁻¹⁷ The phonon effects on the performance of charge qubit are also evaluated in symmetrical DQD system.¹⁸ Generally, there are two important mechanisms constituting decoherence: relaxation and pure dephasing. Relaxation is related to the variation in electron population numbers. In contrast, pure dephasing is related to the loss of phase coherence of the superposition of states. The energy transition among various states is not involved in this mechanism. To understand the role of decoherence in qubit, especially for pure dephasing, extensive works have been devoted to study double and more complex quantum dot systems embedded in bulk environments.¹⁹⁻²² Unlike bulk systems, we aim to investigate the effect of the engineered environment on pure dephasing of charge qubit. It is widely accepted that phonon properties in confined structures are different from those in bulk cases.²³⁻²⁷ Advanced nanotechnology now enables one to design the profile of the structure by altering the dimensions.^{28,29} These promising nanostructures have created a number of interesting properties in electron transport and thermal conductivity.³⁰⁻³²

In this Brief Report, we investigate the pure dephasing of a DQD qubit embedded in a freestanding semiconductor slab. The dephasing source in this qubit comes from the electron-phonon interaction via deformation potential. Two dispersion relations are deduced for phonon properties of the

slab. Density matrix is used to analyze the dynamics of the qubit. By calculating the pure dephasing factor, our results show that the characteristics of phonon modes strongly affect the evolution of the qubit. Because of the confinement, the factor obviously reveals an oscillatory behavior. The effect of individual phonon modes is presented in detail in this research. We also analyze the dependence of temperature on the factor. Moreover, two distinct tendencies are obtained due to particular phonon characteristics.

A double-dot charge qubit is placed in a freestanding semiconductor slab, as shown in Fig. 1. The double-dot structure can be engineered with the help of the external gates.^{28,31} The parameters of confinement potential, such as its magnitude and profile, are precisely modulated via gate voltages.⁵ The confinement configuration can be stably kept under the control of the gates. Most parts of the slab structure are spatially isolated from the support substrate. The in-plane scale of the slab is assumed to exceed substantially the width w and dot radius a . This state ensures that the effect in contact with the substrate can be neglected in the system. The quantum dots are horizontally arranged along the x -axis direction and located at the position z_0 from the center of the slab. To define the logical states of the qubit, we assume that only an additional electron is allowed to exist on the DQD, i.e., an excess electron occupies either the left dot ($|L\rangle$) or the right dot ($|R\rangle$).^{3,33} The total Hamiltonian of the system is

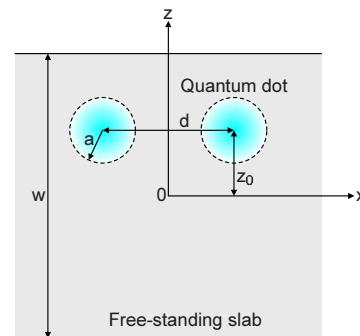


FIG. 1. (Color online) Schematic illustration of a DQD charge qubit embedded in a freestanding slab of width w . Dashed circles represent two identical quantum dots with dot radii a and center-to-center distance d . The positions of two dots are $(\pm d/2, 0, z_0)$ and the surfaces of the slab are $z = \pm w/2$.

$$H = \frac{\varepsilon}{2} \sigma_z + \sum_{\mathbf{q}_{\parallel,n}} \hbar \omega_{\mathbf{q}_{\parallel,n}} b_{\mathbf{q}_{\parallel,n}}^\dagger b_{\mathbf{q}_{\parallel,n}} + \sigma_z \sum_{\mathbf{q}_{\parallel,n}} g_{\mathbf{q}_{\parallel,n}} (b_{\mathbf{q}_{\parallel,n}}^\dagger + b_{-\mathbf{q}_{\parallel,n}}), \quad (1)$$

where the first term is the qubit Hamiltonian, the next term is the phonon bath, and the final term is the electron-phonon interaction. ε is the energy difference and σ_z is the Pauli matrix in the basis of the states $|L\rangle$ and $|R\rangle$. Note that, to capture the main physics of pure dephasing, there is no tunnel coupling between the dots; namely, relaxation mechanism is inhibited. $\omega_{\mathbf{q}_{\parallel,n}}$ is the frequency, $g_{\mathbf{q}_{\parallel,n}}$ is the coupling constant of electrons to phonons, and $b_{\mathbf{q}_{\parallel,n}}^\dagger$ ($b_{\mathbf{q}_{\parallel,n}}$) is the creation (annihilation) operator of the phonons with branch n and in-plane wave vector \mathbf{q}_{\parallel} .

Starting from the elastic continuum model, one can derive the dispersion relation with appropriate boundary conditions.³⁴ The phonon frequency of the slab is obtained via numerical treatment.³⁵ For electron-phonon coupling, the deformation potential is supposed to be the main contributor in our model. For phonon modes allowed to effect, only dilatational waves and flexural waves are contributive. Shear waves are neglected because interaction with electrons vanishes. The phonon frequency is therefore given by^{23,24}

$$\omega_{\mathbf{q}_{\parallel,n}} = s_t \sqrt{q_{\parallel}^2 + q_{t,n}^2} = s_l \sqrt{q_{\parallel}^2 + q_{l,n}^2}, \quad (2)$$

where s_t and s_l are the transverse and longitudinal sound velocities, respectively. The parameters $q_{t,n}$ and $q_{l,n}$ can be evaluated by the equation

$$(q_{\parallel}^2 - q_{t,n}^2)^2 \tan\left(\frac{q_{t,n}w}{2}\right) + 4q_{\parallel}^2 q_{l,n} q_{t,n} \tan\left(\frac{q_{l,n}w}{2}\right) = 0, \quad (3)$$

for the dilatational waves, and

$$(q_{\parallel}^2 - q_{l,n}^2)^2 \tan\left(\frac{q_{l,n}w}{2}\right) + 4q_{\parallel}^2 q_{t,n} q_{l,n} \tan\left(\frac{q_{t,n}w}{2}\right) = 0, \quad (4)$$

for the flexural waves. Referring to the homogeneous approach,³ we derive the corresponding coupling constant which is formulated as

$$g_{\mathbf{q}_{\parallel,n}} = \lambda_{\sigma} P_{\mathbf{q}_{\parallel}} (e^{i\mathbf{q}_{\parallel} \cdot \mathbf{d}/2} - e^{-i\mathbf{q}_{\parallel} \cdot \mathbf{d}/2}), \quad (5)$$

with

$$P_{\mathbf{q}_{\parallel}} = \int d^3\mathbf{r} |\phi(\mathbf{r})|^2 e^{-i\mathbf{q}_{\parallel} \cdot \mathbf{r}_{\parallel}}. \quad (6)$$

Here, λ_{σ} are the coupling functions of the dilatational waves ($\sigma=d$) and flexural waves ($\sigma=f$), and $\phi(\mathbf{r})$ is the electronic wave function in the dot with $\mathbf{r}=(\mathbf{r}_{\parallel}, z)$. For simplicity, the quantum dots are assumed to be isotropic. The wave function of the electron state is modeled by spherical Gaussian function $\phi(\mathbf{r}) = \exp(-r^2/2a^2)/\sqrt{\pi^{3/2}a^3}$. By incorporating the wave function into Eq. (5), we obtain

$$g_{\mathbf{q}_{\parallel,n}} = i\lambda_{\sigma} e^{-\omega_{\mathbf{q}_{\parallel,n}}^2 a^2/4s_t^2} \sin(\mathbf{q}_{\parallel} \cdot \mathbf{d}/2), \quad (7)$$

where

$$\lambda_d = F_d N_n (q_{t,n}^2 - q_{\parallel}^2) (q_{l,n}^2 + q_{\parallel}^2) \sin(q_{t,n}w/2) \cos(q_{l,n}z_0), \quad (8)$$

$$\lambda_f = F_f N_n (q_{t,n}^2 - q_{\parallel}^2) (q_{l,n}^2 + q_{\parallel}^2) \cos(q_{t,n}w/2) \sin(q_{l,n}z_0), \quad (9)$$

with $N_n = \sqrt{\hbar E_a^2/2A\rho\omega_n}$, the normalization constants F_d and F_f , the deformation-potential constant E_a , the area of the slab A , and the mass density ρ .

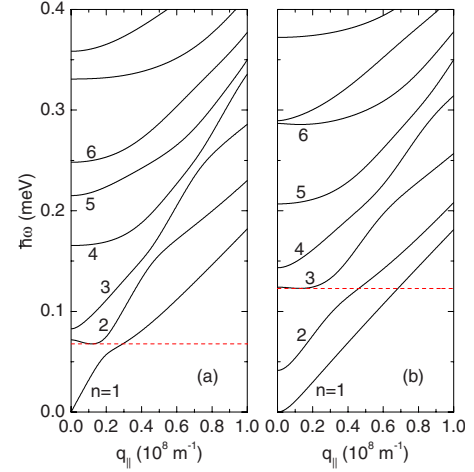


FIG. 2. (Color online) Phonon dispersion relation as a function of wave vector for (a) dilatational waves, and (b) flexural waves in a freestanding slab with width $w=150$ nm. Numbers $n=1$ through 6 are given to label the six lowest branches. Local minima occur on the second dilatational and third flexural branches. The red dashed lines represent the tangent lines to the minimum points.

As the qubit evolves, pure dephasing is induced by the coupling with phonon environment. Such a process destroys the phase information of the qubit. To explore the influence of confined phonons, we calculate the density matrix to determine the pure dephasing of the qubit.^{19,20,36} A general expression of the density matrix can be analytically written as

$$\rho(t) = \begin{pmatrix} \rho_{LL}(0) & \rho_{LR}(0)e^{-\Gamma(t)+iest/\hbar} \\ \rho_{RL}(0)e^{-\Gamma(t)-iest/\hbar} & \rho_{RR}(0) \end{pmatrix}, \quad (10)$$

where the dephasing factor Γ can be considered as a sum of dephasing factors Γ_n of phonon branches n ,

$$\Gamma(t) = \sum_n \Gamma_n(t), \quad (11)$$

$$\Gamma_n(t) = 8 \sum_{\mathbf{q}_{\parallel}} \frac{|g_{\mathbf{q}_{\parallel,n}}|^2}{\hbar^2 \omega_{\mathbf{q}_{\parallel,n}}^2} \sin^2\left(\frac{\omega_{\mathbf{q}_{\parallel,n}} t}{2}\right) \coth\left(\frac{\hbar \omega_{\mathbf{q}_{\parallel,n}}}{2k_B T}\right), \quad (12)$$

with the Boltzmann constant k_B and temperature T . As shown in Eq. (10), the occupations of the states ρ_{LL} and ρ_{RR} keep constant with time. However, the off-diagonal element is dynamically affected by the dephasing factor.

We perform simulations for a freestanding GaAs slab with $E_a=2.2 \times 10^{-18}$ J, $\rho=5.3 \times 10^3$ kg/m³, $s_t=3.0 \times 10^3$ m/s, and $s_l=5.2 \times 10^3$ m/s.³⁷ The related parameters $a=30$ nm, $d=60$ nm, and $w=150$ nm are taken in the model. Unless specified, the temperature is set to be $T=50$ mK. Figure 2 shows the phonon-dispersion relations for dilatational and flexural waves. The curves are not congruous because the related parameters q_{\parallel} , $q_{l,n}$, and $q_{t,n}$ independently satisfy the dispersion relations. The phonon energy has a set of discrete values for each wave vector, resulting in discrete phonon branches. This fact originates from the spatial confinement of the phonons in the z direction. Furthermore, there exists local minima in the second dilatational branch ($n=2$) in Fig. 2(a)

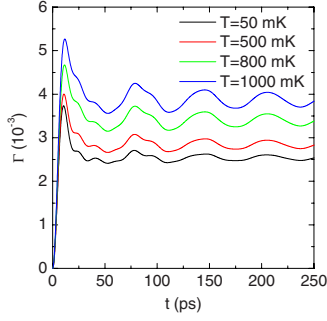


FIG. 3. (Color online) Dephasing factor as a function of time for different temperatures. The dilatational waves are only considered because the double dot is located at the center of the slab ($z_0 = 0$ nm).

and the third flexural branch ($n=3$) in Fig. 2(b), respectively. To emphasize this finding, we plot the horizontal tangent lines to the branches at the minimum points ($\hbar\omega_p$), which correspond to 0.068 and 0.122 meV. For a slab, the phonon density of states can be defined as

$$\rho(\omega) = \sum_n \sum_{\mathbf{q}_{\parallel}} \delta(\omega - \omega_{\mathbf{q}_{\parallel},n}). \quad (13)$$

Since the density of states depends on $1/|\partial\omega_{\mathbf{q}_{\parallel},n}/\partial q_{\parallel}|$, the phonon van Hove singularities occur at the points ($\partial\omega_{\mathbf{q}_{\parallel},n}/\partial q_{\parallel}=0$).^{24,38} Accordingly, these remarkable phonon properties are expected to strongly affect the dephasing of the qubit.

We consider that the DQD is located at the center of the slab. Due to the symmetry, the flexural waves do not contribute effects to the dephasing of the system [Eq. (9)]. Figure 3 shows the dephasing factor for the dilatational waves. The curves rapidly increase in the beginning. After that, the curves show an interesting oscillation. Unlike monotonic behavior in bulk systems, such a crucial feature results from the phonon confinement effect. As the qubit continuously evolves, the oscillation will be obviously suppressed in long-time duration. In the limit of $t \rightarrow \infty$, we can average the oscillating term, $\sin^2(\omega_{\mathbf{q}_{\parallel},n}t/2) \rightarrow 1/2$. The dephasing factor $\Gamma(t \rightarrow \infty)$ asymptotically approaches a constant, which is given by

$$\Gamma(t \rightarrow \infty) = 4 \sum_n \sum_{\mathbf{q}_{\parallel}} \frac{|g_{\mathbf{q}_{\parallel},n}|^2}{\hbar^2 \omega_{\mathbf{q}_{\parallel},n}^2} \coth\left(\frac{\hbar\omega_{\mathbf{q}_{\parallel},n}}{2k_B T}\right). \quad (14)$$

At $T=50$ mK, the magnitude of $\Gamma(t \rightarrow \infty)$ is estimated to be 2.54×10^{-3} . The effect of temperature on the dephasing is also shown. As high temperature leads to an increasing in phonon occupation, the magnitude of the dephasing factor is enhanced. This effective phenomenon enlarges the loss of coherence in the qubit.

To clarify the above consequence, we analyze the contribution of individual phonon branch to the dephasing. Figure 4 depicts the contribution of the six lowest branches for the dilatational waves. As seen in Eq. (7), the contribution from high-energy phonon branches is suppressed by the factor s_l/a , which corresponds to an energy of 0.11 meV. In short-time duration, the trigonometric function $\sin(\omega_{\mathbf{q}_{\parallel},n}t/2)$ domi-

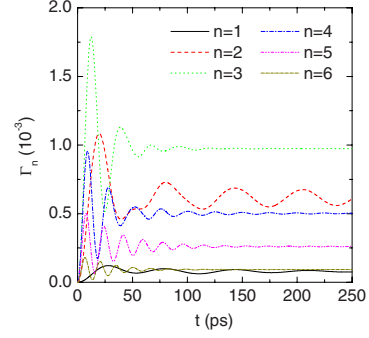


FIG. 4. (Color online) Time evolution of the dephasing factor Γ_n for different branches n of the dilatational waves.

ates the function $\Gamma_n(t)$. For these branches the time evolutions of Γ_n are in the same directional phase, leading to a strong increase of dephasing factor. Interestingly, one can find that the second branch ($n=2$) provides a significant influence on the oscillating behavior, as shown in Fig. 4. By analyzing the revival of recovered activation, its frequency approaches to the energy scale $\hbar\omega_p$, which corresponds to the minimum of the second branch shown in Fig. 2(a). Consequently, the fact that a high density of states appears at the point remarkably modifies the dynamics of the dephasing.

The DQD is subsequently placed at the position $z_0 = 30$ nm, separated from the center of the slab. In addition to dilatational waves, flexural waves become an important contributor. The sum of dephasing factors is derived from the subtotal dephasing rates induced by two waves. Owing to the varied dispersion relations, two evolutions of dilatational and flexural waves are typically shown in Fig. 5. One can find the rate of the dephasing factor for the flexural wave is faster than that for the dilatational waves in short-time duration. For very short time ($t \rightarrow 0$), the dephasing factor becomes

$$\Gamma(t) \approx 2t^2 \sum_n \sum_{\mathbf{q}_{\parallel}} \frac{|g_{\mathbf{q}_{\parallel},n}|^2}{\hbar^2} \coth\left(\frac{\hbar\omega_{\mathbf{q}_{\parallel},n}}{2k_B T}\right). \quad (15)$$

According to Eq. (15), the ratio in dephasing factor of flexural and dilatational waves is roughly 1.8:1 in this case. The dephasing channel depends more on the flexural waves than the dilatational waves. As seen in Fig. 6, the faster growing

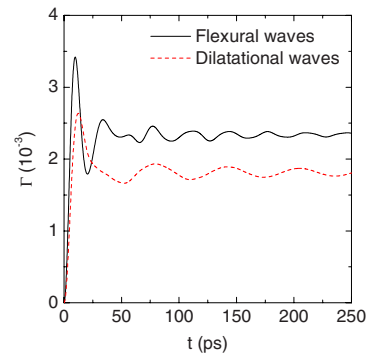


FIG. 5. (Color online) Dephasing factor as a function of time for the dilatational and flexural waves. The position of double dot is set to be $z_0 = 30$ nm.

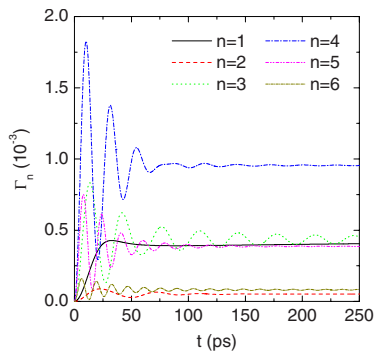


FIG. 6. (Color online) Time evolution of the dephasing factor Γ_n for different branches n of the flexural waves at the position $z_0 = 30$ nm.

activation is attributed to higher-energy flexural branches. During the subsequent longer time, one again observes a nearly similar oscillation for the flexural waves as shown in Fig. 5. Specifically, the frequency of the curve is different from that for the dilatational waves. As shown in Fig. 6, the dephasing factor Γ_3 contributes extremely strong influence to the oscillation. The origin of the revival mainly results from the phonon van Hove singularity for the flexural waves.

Some comparisons with the related studies should be addressed here. Quantum coherence is an important issue for the qubit performance.^{39–41} As the qubit is embedded in a bulk environment, the dephasing shows some similar results.^{19,20} In other words, the interaction between the qubit

and bulk acoustic phonons leads to a fast increase of dephasing. Furthermore, it smoothly evolves and saturates to a non-zero value. The related results are also explored in spin and exciton systems.^{42,43} The magnitude of dephasing depends on the temperature, structure and material parameters. In our model, however, the decoherence reveals particular features which do not occur in bulk cases. The time evolution of dephasing exhibits an oscillating dynamics due to the singular phonon density of states for the slab. Since the characteristic is intrinsic, such an oscillating feature can also be observed for different temperatures. According to the results studied above, one can expect that the distinctive signature still appears in the dephasing dynamics of multiqubit systems embedded in a freestanding slab.^{21,22,44}

We have investigated pure dephasing in a DQD charge qubit placed in a freestanding slab. The dispersion relations are calculated for different phonon modes in the confined environment. By calculating the density matrix, our result indicates that the dephasing factor reveals a nonmonotonic evolution. The contribution of particular phonon modes is exploited. Moreover, we have studied the determined value of the temperature dependence, corresponding to the dephasing factor. Specifically, pronounced oscillations are clearly observed as a result of phonon confinement effect.

This work was supported by the National Science Council, Taiwan under Grants No. NSC 97-2112-M-390-006-MY3 and No. 98-2112-M-006-002-MY3.

*yyliao@nuk.edu.tw

¹D. Loss and D. P. DiVincenzo, *Phys. Rev. A* **57**, 120 (1998).

²T. Tanamoto, *Phys. Rev. A* **61**, 022305 (2000).

³T. Brandes, *Phys. Rep.* **408**, 315 (2005).

⁴S. M. Reimann and M. Manninen, *Rev. Mod. Phys.* **74**, 1283 (2002).

⁵W. G. van der Wiel *et al.*, *Rev. Mod. Phys.* **75**, 1 (2002).

⁶T. Hayashi *et al.*, *Phys. Rev. Lett.* **91**, 226804 (2003).

⁷J. R. Petta, *et al.*, *Phys. Rev. Lett.* **93**, 186802 (2004).

⁸J. Gorman *et al.*, *Phys. Rev. Lett.* **95**, 090502 (2005).

⁹L. Viola and S. Lloyd, *Phys. Rev. A* **58**, 2733 (1998).

¹⁰B. Krummheuer *et al.*, *Phys. Rev. B* **65**, 195313 (2002).

¹¹M. J. Storcz *et al.*, *Phys. Rev. B* **72**, 235321 (2005).

¹²Z. J. Wu *et al.*, *Phys. Rev. B* **71**, 205323 (2005).

¹³S. Vorobjov *et al.*, *Phys. Rev. B* **71**, 205322 (2005).

¹⁴M. Thorwart *et al.*, *Phys. Rev. B* **72**, 235320 (2005).

¹⁵K. Roszak and P. Machnikowski, *Phys. Rev. A* **73**, 022313 (2006).

¹⁶Y. Y. Liao, Y. N. Chen, W. C. Chou, and D. S. Chuu, *Phys. Rev. B* **77**, 033303 (2008).

¹⁷W. M. Ju *et al.*, *Eur. Phys. J. B* **72**, 417 (2009).

¹⁸L. Fedichkin *et al.*, *Nanotechnology* **11**, 387 (2000).

¹⁹L. Fedichkin and A. Fedorov, *Phys. Rev. A* **69**, 032311 (2004).

²⁰V. N. Stavrou and X. Hu, *Phys. Rev. B* **72**, 075362 (2005).

²¹W. Ben Chouikha, S. Jaziri, and R. Bennaceur, *Phys. Rev. A* **76**, 062303 (2007).

²²R. Doll, M. Wubs, P. Hänggi, and S. Kohler, *Phys. Rev. B* **76**, 045317 (2007).

²³N. Bannov *et al.*, *Phys. Rev. B* **51**, 9930 (1995).

²⁴A. Balandin and K. L. Wang, *Phys. Rev. B* **58**, 1544 (1998).

²⁵J. Zou and A. Balandin, *J. Appl. Phys.* **89**, 2932 (2001).

²⁶Y. Y. Liao, Y. N. Chen, D. S. Chuu, and T. Brandes, *Phys. Rev. B* **73**, 085310 (2006).

²⁷D. L. Nika *et al.*, *Appl. Phys. Lett.* **93**, 173111 (2008).

²⁸E. M. Höhberger *et al.*, *Appl. Phys. Lett.* **82**, 4160 (2003).

²⁹E. M. Weig *et al.*, *Phys. Rev. Lett.* **92**, 046804 (2004).

³⁰L. Donetti *et al.*, *J. Appl. Phys.* **100**, 013701 (2006).

³¹C. Rossler *et al.*, *Nanotechnology* **19**, 165201 (2008).

³²K. Sun *et al.*, *J. Appl. Phys.* **105**, 074316 (2009).

³³Y. Y. Liao, D. S. Chuu, and Y. N. Chen, *Phys. Rev. B* **75**, 125325 (2007).

³⁴B. A. Auld, *Acoustic Fields and Waves in Solids* (Wiley, New York, 1973).

³⁵J. Zou, *Am. J. Phys.* **76**, 460 (2008).

³⁶D. Mozyrsky and V. Privman, *J. Stat. Phys.* **91**, 787 (1998).

³⁷H. Bruus *et al.*, *Phys. Rev. B* **48**, 11144 (1993).

³⁸S. Debald *et al.*, *Phys. Rev. B* **66**, 041301(R) (2002).

³⁹R. Doll *et al.*, *Eur. Phys. J. B* **68**, 523 (2009).

⁴⁰D. Culcer *et al.*, *Appl. Phys. Lett.* **95**, 073102 (2009).

⁴¹J. Fischer *et al.*, *Solid State Commun.* **149**, 1443 (2009).

⁴²K. Roszak and P. Machnikowski, *Phys. Rev. B* **80**, 195315 (2009).

⁴³T. E. Hodgson, L. Viola, and I. D'Amico, *Phys. Rev. B* **78**, 165311 (2008).

⁴⁴D. Solenov, D. Tolkunov, and V. Privman, *Phys. Rev. B* **75**, 035134 (2007).